Variability of Transrectal Shear Wave Elastography in a Phantom Model

팬텀연구에서 경직장 전단파탄성초음파의 가변성

Jihyun Lee, MD[1] (iD), Seong Kuk Yoon, MD[2]* (iD), Jin Han Cho, MD[2] (iD), Hee Jin Kwon, MD[2] (iD), Dong Won Kim, MD[3] (iD), Jun Woo Lee, MD[4] (iD)

[1]Department of Radiology, Dongnam Institute of Radiological and Medical Science, Busan, Korea
[2]Department of Radiology, Dong-A University College of Medicine, Dong-A University Hospital, Busan, Korea
[3]Department of Radiology, Isam Hospital, Busan, Korea
[4]Department of Radiology, Pusan National University Yangsan Hospital, Yangsan, Korea

*Corresponding author
Seong Kuk Yoon, MD
Department of Radiology,
Dong-A University
College of Medicine,
Dong-A University Hospital,
26 Daesingongwon-ro, Seo-gu,
Busan 49201, Korea.

Tel 82-51-240-5367
Fax 82-51-253-4931
E-mail skyoon@dau.ac.kr

ORCID iDs
Jihyun Lee (iD) https://orcid.org/0000-0001-8198-9241
Seong Kuk Yoon (iD) https://orcid.org/0000-0001-7182-1701
Jin Han Cho (iD) https://orcid.org/0000-0002-5929-9399
Hee Jin Kwon (iD) https://orcid.org/0000- 0002-2001-953X
Dong Won Kim (iD) https://orcid.org/0000-0003-0207-9587
Jun Woo Lee (iD) https://orcid.org/0000-0002-7701-9012

Purpose This study aimed to assess the variability of transrectal shear wave elastography (SWE) using a designed phantom.
Materials and Methods In a phantom, the SWE values were examined by two radiologists using agarose and emulsion silicone of different sizes (1, 2, and 3 cm) and shapes (round, cubic) at three depths (1, 2, and 3 cm), two region of interest (ROI) and locations (central, peripheral) using two ultrasound machines (A, B from different vendors). Variability was evaluated using the coefficient of variation (CV).
Results The CVs decreased with increasing phantom size. Significant changes in SWE values included; agarose phantom at 3 cm depth ($p < 0.001$; machine A), 1 cm depth ($p = 0.01$; machine B), emulsion silicone at 2 cm depth ($p = 0.047$, $p = 0.020$; both machines). The CVs increased with increasing depth. Significant changes in SWE values included; 1 cm agarose ($p = 0.037$, $p = 0.021$; both machines) and 2 cm agarose phantom ($p = 0.047$; machine A). Significant differences in SWE values were observed between the shapes for emulsion silicone phantom ($p = 0.032$; machines A) and between ROI locations on machine B ($p \leq 0.001$). The SWE values differed significantly between the two machines ($p < 0.05$). The intra-/inter-operator agreements were excellent (intraclass correlation coefficient > 0.9).
Conclusion The phantom size, depth, and different machines affected the variability of transrectal SWE.

Index terms Elastography; Ultrasound; Prostate; Tissue Elasticity Imaging

INTRODUCTION

Prostate cancer is the second most common malignancy in male (1). The current methods for prostate cancer detection include a digital rectal examination, serum prostate-specific antigen (PSA) levels and transrectal ultrasound (US) with biopsy. A prostate biopsy is performed if the PSA level or digital rectal examination is abnormal (2). However, US-guided transrectal biopsies are prone to sampling errors, missing or under-diagnosed aggressive tumors and detection of indolent cancers that may not require immediate treatment (3). Increasing the number of biopsy cores could improve the cancer detection rate. However, this could result in over-diagnosis of clinically insignificant cancers and increase the risk of biopsy-related complications (4). Although multi-parameter MRI has become a major modality for tumor detection, localization and staging, its specificity remains low (5, 6).

Conventional US has limited sensitivity and specificity between 40% and 50% for prostate cancer detection and is not significantly improved using Color/Power Doppler US (7). One of the advanced US techniques, US elastography, enables differentiation between benign and malignant lesions based on their stiffness (8). Shear wave elastography (SWE), a relatively new type of US elastography, is based on the measurement of shear wave velocity propagating through the tissues and provides quantitative values of prostate stiffness in kilopascals (kPa) (9).

Several studies have investigated the role of SWE in prostate cancer diagnosis. Despite the promising results of initial studies, subsequent studies have reported variable diagnostic performance to reliably differentiate between benign and malignant prostate tissue (10-12). To date, the factors affecting transrectal SWE measurements have not been systematically studied. It is essential to evaluate the variability of SWE and understand the factors associated with inconsistent measurements that may influence its reliability. Therefore, this study aimed to assess the variability of transrectal SWE measurements using a designed phantom.

MATERIALS AND METHODS

This study did not require approval from the Institutional Review Board because it did not involve any humans/animals.

PHANTOM FABRICATION

A phantom was designed to evaluate the elastic properties of soft tissue-mimicking materials for SWE. A phantom container ($15 \times 18 \times 15$ cm³) was fabricated using acrylic plastic material, and an opening was prepared for the US transducer on the wall (Fig. 1). The phantom container was filled with water-based scanning gels. The materials included agarose and emulsion silicone, and the inclusions were placed in the phantom container at specific locations. Inclusions of different sizes and shapes were made using molds that were created with 3D-printed PLA and silicone. The spherical mold consisted of two halves with several cavities of different diameters, and the cubic mold consisted of several cavities of different lengths (Fig. 2). Each phantom material was prepared as three round lesions of different diameters (1, 2, and 3 cm) and three cubic lesions of different lengths (1, 2, and 3 cm) (Fig. 3). Agarose powder in solution was heated and stirred at a temperature above 95℃, subsequently poured
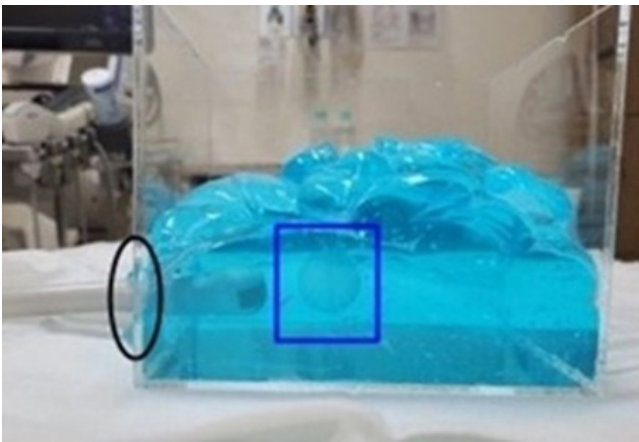
Fig. 1. Designed elastography phantom model.
The image shows the designed prostate phantom. The circle indicates the opening for the transrectal US transducer, and the square indicates the phantom inclusion. The phantom container is filled with water-based scanning gels.

Fig. 2. 3D-printed molds to manufacture the phantom inclusion.
The spherical mold consists of two halves with several cavities of different diameters (1, 2, and 3 cm), and the cubic mold consists of several cavities of different lengths (1, 2, and 3 cm).

Fig. 3. Prepared phantom inclusions in different sizes and shapes.
A, B. Each phantom material was prepared as three round lesions of different diameters (1, 2, and 3 cm) and three cubic lesions of different lengths (1, 2, and 3 cm); agarose (A) emulsion silicone (B).
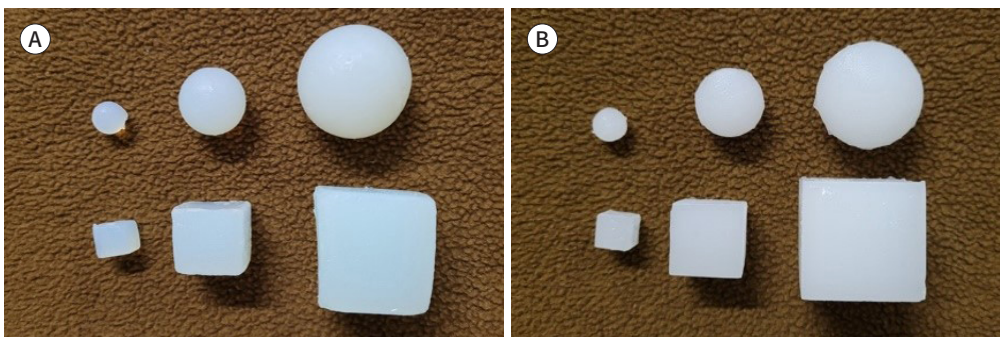
into the silicone mold for cooling, 3% agarose gel inclusion was prepared. Emulsion silicone is silicone mixed with 30% mineral oil to improve acoustic properties with less attenuation than pure silicone (13). The casting process of the emulsion silicone phantom consisted of mixing one-part condensation cure products and mineral oil. It was then poured into 3D-printed molds and cured for 4 hours at room temperature.

TRANSRECTAL SWE AND DATA ACQUISITION

Two US machines equipped with SWE modes were used: General Electric LOGIQ E10 (GE

Healthcare, Milwaukee, IL, USA; machine A) using a transrectal 5–9 MHz transducer and Canon Aplio i800 (Canon Medical Systems Corp., Otawara, Tochigi, Japan; machine B) using a transrectal 3–10 MHz transducer. Machine B also displayed a propagation map revealing the shear wave arrival time contour and served as quality control. The measurement protocol recommended placing a region of interest (ROI) in the area with the most parallel propagation contours (14).

In the phantom container, the transducer was positioned parallel to the phantom inclusion at depths of 1, 2, and 3 cm (Fig. 1). The depth from the transducer was defined as the shortest depth from the transducer to the surface of the phantom. The SWE ROI was placed at the center and periphery of the inclusion. ROI location was interpreted as "central" when ROI was placed in the center within the inclusion and as "peripheral" when located at the right outer half within the inclusion. Both ROIs had as similar depths from the transducer as possible. The ROI used for all measurements was round, and its diameter ranged from 3–5 mm to avoid counting background stiffness (Fig. 4). The transducer was replaced between the acquisitions. Two board-certified radiologists measured the phantom SWE values. Each operator acquired a reading that was blinded to the others. Two types of phantoms with different sizes (1, 2, and 3 cm) and shapes (round, cubic) were measured three times at three depths (1, 2, and 3 cm), two ROI locations (central, peripheral) by two operators. A total of 864 measurements were acquired for both machines.

STATISTICS

Statistical analyses were performed using the SPSS version 23 (IBM Corp., Armonk, NY, USA). The coefficient of variation (CV) was used to describe the measurement variability, calculated as the standard deviation divided by the mean stiffness and expressed as a percentage, with a higher CV indicating higher variability. For continuous values, normality was assessed using the Shapiro–Wilk test. Since the hypothesis of normality was rejected, the Kruskal-Wallis test was used to compare the SWE values according to phantom size and depth. Because phantom size and depth are well-known as the main factors influencing SWE values, the one-way analysis of covariance (ANCOVA) was used to compare SWE values according to

Fig. 4. SWE measurement obtained using two different US systems.
A. The SWE images show 1 cm round shape, emulsion silicone phantom inclusion acquired at a depth of 2 cm using machine A.
B. The SWE images show 1 cm round shape, emulsion silicone phantom inclusion acquired at a depth of 1 cm using machine B.
SWE = shear wave elastography
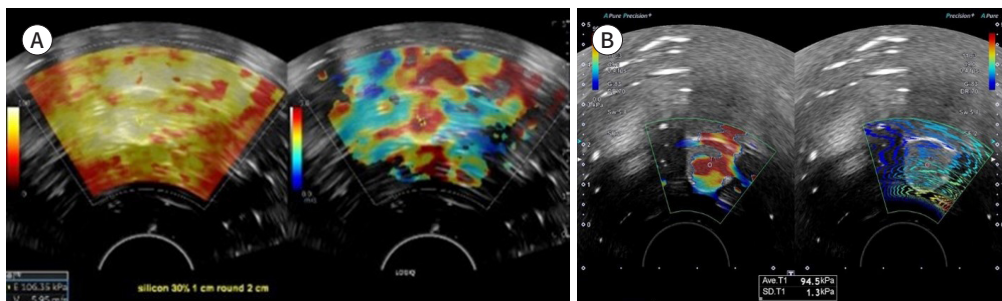
the inclusion shape and ROI location with adjustments for size and depth. Independent *t*-test analysis was applied to assess the inter-machine difference between the two machines. Additionally, the intraclass correlation coefficient (ICC) was used to assess intra- and inter-operator variability by evaluating measurements, with a higher ICC indicating excellent agreement. A $p < 0.05$ was regarded as indicating statistical significance.

RESULTS

EFFECT OF PHANTOM INCLUSION SIZE ON SWE MEASUREMENT

For each phantom with different sizes and depths from the transducer, 48 measurements were taken with machines A ($n = 24$) and B ($n = 24$). The SWE values measured at the same depths (1, 2, and 3 cm) were compared, and the shape of the phantom, ROI location and operator were not considered. As shown in Table 1 and Fig. 5, the CVs decreased according to the phantom size in most agarose phantoms. For the emulsion silicone phantom, the CVs measured at each depth decreased gradually with increasing phantom size in most cases. In contrast, the CV measured at a depth of 3 cm on machine B decreased and then slightly increased (Fig. 6).

Regarding the SWE values, there were significant differences according to inclusion size for the agarose phantom measured at a depth of 3 cm on machine A ($p < 0.001$) and 1 cm on machine B ($p = 0.010$) and for the emulsion silicone phantom measured at a depth of 2 cm on

Table 1. Descriptive Summary of Mean Stiffness Values (kPa) and Variability according to the Size and Depth of Phantom Materials

Phantom Material			Machine A		Machine B	
Type	Size (cm)	Depth (cm)	Mean ± SD (kPa)	CV (%)	Mean ± SD (kPa)	CV (%)
Agarose	1	1	13.0 ± 2.5	19.4	32.5 ± 2.6	7.9
		2	12.9 ± 2.9	22.4	33.5 ± 2.7	8.1
		3	15.2 ± 3.5	22.9	34.9 ± 3.7	10.6
	2	1	12.4 ± 2.2	17.9	34.6 ± 2.4	7.0
		2	11.5 ± 2.3	19.6	35.3 ± 2.8	8.0
		3	10.6 ± 2.3	21.6	35.2 ± 3.9	11.0
	3	1	11.4 ± 2.4	21.3	33.9 ± 2.4	7.1
		2	11.4 ± 2.2	19.3	34.3 ± 3.4	9.8
		3	12.1 ± 3.4	28.3	33.9 ± 3.6	10.5
Emulsion silicone	1	1	113.4 ± 16.1	14.2	121.1 ± 10.8	8.9
		2	113.9 ± 20.9	18.3	114.5 ± 13.1	11.5
		3	123.5 ± 24.5	19.8	123.8 ± 15.6	12.9
	2	1	119.0 ± 14.0	11.7	122.3 ± 10.3	8.4
		2	120.3 ± 11.9	9.9	122.6 ± 9.2	7.5
		3	122.9 ± 17.2	14.0	128.5 ± 12.4	9.8
	3	1	118.2 ± 8.9	7.5	125.3 ± 8.0	6.4
		2	120.8 ± 10.5	8.7	125.3 ± 9.0	7.2
		3	122.6 ± 16.0	13.0	122.2 ± 12.8	10.5

CV = coefficient of variation, SD = standard deviation

Fig. 5. Comparison of stiffness value of the agarose phantom according to the phantom sizes and different depths. The graph represents the mean stiffness value and 95% CIs according to the phantom size and depth for each machine. *On machine A, there were significant differences according to inclusion size for the agarose phantom measured at a depth of 3 cm ($p < 0.001$). There were significant changes with increasing depth for the 1 cm agarose phantom ($p = 0.037$) and the 2 cm phantom ($p = 0.047$). On machine B, there were significant differences according to inclusion size for the agarose phantom measured at a depth of 1 cm ($p = 0.010$). There were significant changes with increasing depth for the 1 cm agarose phantom ($p = 0.02$). CI = confidence interval
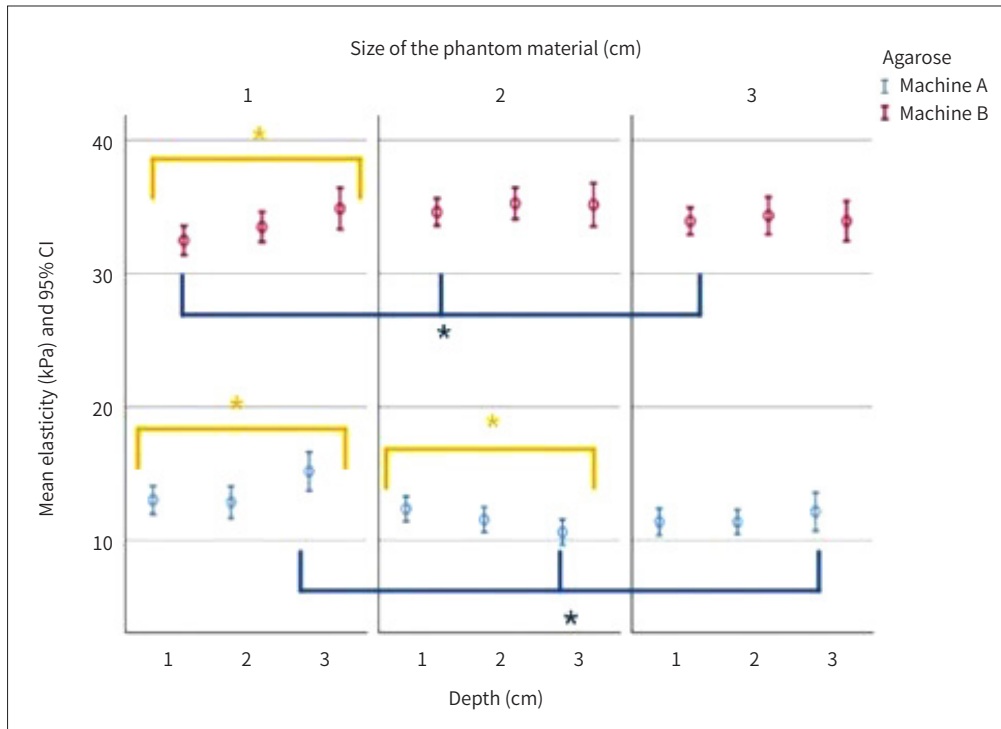
both machines (machine A, $p = 0.047$; machine B, $p = 0.020$). No significant difference was found in the SWE value for the agarose phantom at depths of 1 cm (machine A, $p = 0.111$), 2 cm (machine A, $p = 0.197$; machine B, $p = 0.060$), and 3 cm (machine B, $p = 0.470$). For the emulsion silicone phantom, there was no association between SWE values and phantom size at depths of 1 cm (machine A, $p = 0.392$; machine B, $p = 0.130$) and 3 cm (machine A, $p = 0.984$; machine B, $p = 0.213$).

EFFECT OF THE DEPTH ON SWE MEASUREMENT

The SWE values measured at the same size as the phantom (1, 2, and 3 cm) were compared using two machines without considering the shape of the phantom, ROI location, or operator. A summary of the results between depths is presented in Table 1. The CVs showed an increasing tendency as the depth increased. From 1 to 3 cm agarose phantom, the CVs gradually increased with increasing depth on both machines except for the 3 cm agarose phantom on machine A. For the 3 cm agarose phantom, the CV at a depth of 2 cm was slightly lower than that at 1 cm on machine A; however, the CV at a depth of 3 cm increased with acquisition depth (Fig. 5). For the 1- and 3 cm emulsion silicone phantoms, the CVs at all depths gradually increased on both machines. For the 2 cm emulsion silicone phantom, the CVs at a

Fig. 6. Comparison of stiffness value of the emulsion silicone phantom according to the phantom sizes and different depths. The graph represents the mean stiffness value and 95% CIs according to the phantom size and depth for each machine. *There were significant differences according to inclusion size for the emulsion silicone phantom measured at a depth of 2 cm both machines (machine A, p = 0.047; machine B, p = 0.020). CI = confidence interval
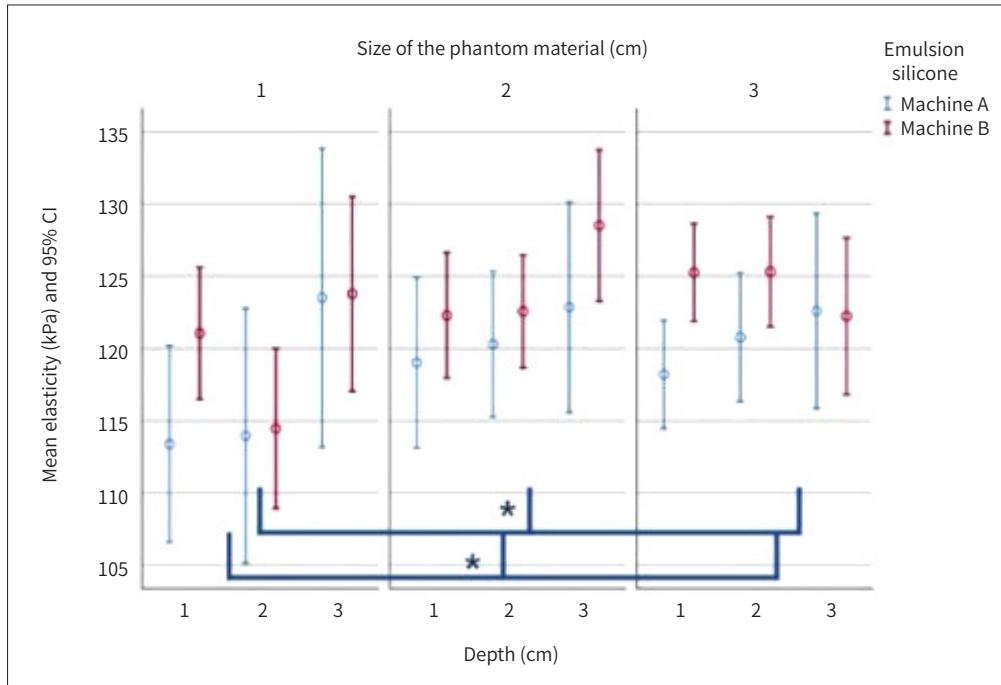
depth of 2 cm were slightly lower than those at 1 cm on both machines, but the CVs at a depth of 3 cm increased with acquisition depth (Fig. 6).

Regarding the SWE value, there were significant changes with increasing depth for the 1 cm agarose phantom (machine A, p = 0.037; machine B, p = 0.021) and the 2 cm phantom (machine A, p = 0.047). The SWE values of the agarose phantom sized 2 cm (machine B, p = 0.509) and 3 cm (machine A, 0.718; machine B, p = 0.756) did not reach statistical significance with depth. For emulsion silicone phantoms of three different sizes, the SWE values at different depths were not significantly different for both machines (machine A, p = 0.329 [1 cm], p = 0.810 [2 cm] and p = 0.489 [3 cm]; machine B, p = 0.096 [1 cm], p = 0.187 [2 cm], p = 0.402 [3 cm]).

EFFECT OF PHANTOM SHAPE ON SWE MEASUREMENT

For each phantom with different shapes, sizes and depths from the transducer, 24 measurements were performed using machines A (n = 12) and B (n = 12). SWE values measured at the same depth and size were compared, and the ROI location or operator was not considered. A summary of the phantom shape results is presented in Table 2. There was no association between the variability and phantom shape. The results demonstrated that no significant difference in SWE values was found between round and cubic shapes (agarose, p = 0.154 and p = 0.541 on both machines, respectively; emulsion silicone, p = 0.388 on machine B), whereas there was a significant difference between shapes for the emulsion silicone phantom obtained using machine A (p = 0.032).

Table 2. Impact of Phantom Material and Shape on Stiffness Values and Variability of Shear Wave Elastography

Phantom			Machine A				Machine B			
	Shape		Round		Cubic		Round		Cubic	
Type	Size (cm)	Depth (cm)	Mean ± SD (kPa)	CV (%)	Mean ± SD (kPa)	CV (%)	Mean ± SD (kPa)	CV (%)	Mean ± SD (kPa)	CV (%)
Agarose	1	1	12.6 ± 2.7	21.2	13.4 ± 2.4	18.1	33.7 ± 2.9	8.6	31.2 ± 1.5	4.9
		2	11.7 ± 1.8	15.4	14.0 ± 3.4	24.1	33.7 ± 2.5	7.4	33.3 ± 3.0	9.1
		3	15.3 ± 3.8	24.9	15.0 ± 3.3	21.7	34.6 ± 3.9	11.1	35.2 ± 3.7	10.5
	2	1	11.6 ± 2.2	18.8	13.1 ± 2.1	15.8	33.8 ± 2.8	8.4	35.4 ± 1.7	4.9
		2	11.3 ± 2.4	21.6	11.8 ± 2.2	18.3	35.0 ± 2.8	8.1	35.5 ± 2.9	8.3
		3	10.2 ± 2.0	19.4	11.0 ± 2.6	23.4	34.1 ± 4.7	13.8	36.2 ± 2.5	7.0
	3	1	11.1 ± 2.6	23.4	11.7 ± 2.3	19.4	34.9 ± 2.8	7.9	33.0 ± 1.6	4.9
		2	11.1 ± 2.5	22.8	11.7 ± 1.9	16.2	33.4 ± 3.2	9.6	35.2 ± 3.4	9.7
		3	13.2 ± 3.7	27.8	11.1 ± 3.0	27.2	33.7 ± 2.9	8.7	34.1 ± 4.2	12.4
Emulsion silicone	1	1	112.0 ± 17.2	15.4	114.8 ± 15.5	13.5	119.9 ± 10.6	8.8	122.2 ± 3.0	9.3
		2	107.2 ± 9.9	9.2	120.7 ± 26.8	22.2	114.8 ± 16.6	14.5	114.1 ± 9.1	8.0
		3	111.2 ± 18.7	16.7	135.8 ± 24.0	17.7	124.6 ± 15.9	12.7	123.0 ± 16.7	13.6
	2	1	116.0 ± 13.6	11.7	122.1 ± 14.3	11.7	125.4 ± 10.3	8.2	119.1 ± 9.7	8.1
		2	124.0 ± 10.6	8.6	116.5 ± 12.4	10.7	125.4 ± 8.1	6.4	119.8 ± 9.8	8.2
		3	119.1 ± 16.2	13.6	126.6 ± 18.2	14.3	127.9 ± 13.9	10.9	129.1 ± 11.3	8.8
	3	1	122.2 ± 9.8	8.0	114.2 ± 5.7	5.0	121.6 ± 7.1	5.8	128.9 ± 7.4	5.8
		2	118.6 ± 11.4	9.6	122.2 ± 9.6	7.8	122.3 ± 8.3	6.8	128.3 ± 9.0	7.0
		3	123.0 ± 17.5	14.2	122.2 ± 15.0	12.3	117.3 ± 6.9	5.9	127.2 ± 15.6	12.3

CV = coefficient of variation, SD = standard deviation

EFFECT OF ROI LOCATION ON SWE MEASUREMENT

For each phantom material with different ROI locations, phantom sizes and depths from the transducer, 24 measurements were performed using machines A (n = 12) and B (n = 12). SWE values measured at the same depth and size were compared without considering the shape or operator. As shown in Table 3, there was no association between the variability and ROI location of each phantom. For both inclusions obtained using machine B, there were significant differences in the stiffness values between different ROI locations (agarose, p = 0.001; emulsion silicone p < 0.001), demonstrating that the mean SWE value of the centrally located ROI was slightly higher than that of the peripherally located ROI. Machine A had no significant difference in the stiffness value according to the ROI location (agarose, p = 0.532; emulsion silicone, p = 0.314).

COMPARISON OF SWE MEASUREMENTS BETWEEN THE MACHINES AND OPERATORS

The measured SWE values between the machines differed significantly for both phantom materials (agarose, p < 0.001; emulsion silicone, p = 0.013). The mean differences (95% confidence interval [CI]) of SWE values between the two machines were -21.95 kPa (-22.52 to -21.38) for the agarose phantom and, while the mean differences were -3.42 kPa (-6.12 to -0.73) for the emulsion silicone phantom. The differences between the machines were more

Table 3. Impact of ROI Location on Stiffness Values and Variability of Shear Wave Elastography

Phantom Material			Machine A				Machine B			
			Central ROI		Peripheral ROI		Central ROI		Peripheral ROI	
Type	Size (cm)	Depth (cm)	Mean ± SD (kPa)	CV (%)	Mean ± SD (kPa)	CV (%)	Mean ± SD (kPa)	CV (%)	Mean ± SD (kPa)	CV (%)
Agarose	1	1	12.4 ± 2.4	19.3	13.6 ± 2.6	19.3	32.8 ± 2.6	7.9	32.1 ± 2.7	8.3
		2	12.6 ± 2.9	23.2	13.1 ± 3.0	22.5	34.4 ± 3.1	9.0	32.6 ± 2.0	6.0
		3	15.6 ± 3.0	19.5	14.8 ± 4.0	26.8	35.9 ± 2.8	7.8	33.8 ± 4.3	12.7
	2	1	12.3 ± 1.4	11.7	12.4 ± 2.9	23.1	34.7 ± 2.5	7.1	34.5 ± 2.5	7.3
		2	11.9 ± 2.6	21.6	11.2 ± 2.0	17.6	36.2 ± 2.1	5.8	34.3 ± 3.2	9.4
		3	11.1 ± 2.7	24.5	10.0 ± 1.7	16.6	35.3 ± 3.0	8.6	35.0 ± 4.7	13.4
	3	1	11.7 ± 2.7	23.2	11.0 ± 2.2	19.6	34.8 ± 2.5	7.2	33.0 ± 2.1	6.4
		2	10.6 ± 2.0	19.2	12.2 ± 2.2	17.7	35.6 ± 3.8	10.7	33.1 ± 2.4	7.3
		3	13.3 ± 3.4	25.9	11.0 ± 3.1	28.7	34.7 ± 3.9	11.2	33.1 ± 3.2	9.5
Emulsion silicone	1	1	117.9 ± 14.7	12.4	108.8 ± 16.8	15.4	124.3 ± 12.8	10.3	117.8 ± 7.6	6.4
		2	120.6 ± 25.3	21.0	107.4 ± 13.3	12.4	115.7 ± 9.0	7.7	113.3 ± 16.6	14.7
		3	123.8 ± 25.4	20.5	123.2 ± 24.7	20.1	131.8 ± 14.5	11.0	115.8 ± 13.5	11.7
	2	1	116.3 ± 9.0	18.0	121.7 ± 17.7	14.5	124.7 ± 11.8	9.5	119.8 ± 8.3	6.9
		2	122.6 ± 11.7	9.5	118.0 ± 11.7	10.4	127.4 ± 8.7	6.8	117.7 ± 7.2	6.1
		3	126.0 ± 16.4	13.0	119.7 ± 18.2	15.2	132.7 ± 13.6	10.2	124.3 ± 10.1	8.1
	3	1	117.9 ± 8.5	7.2	118.5 ± 9.6	8.1	128.8 ± 6.7	5.2	121.7 ± 7.8	6.4
		2	123.0 ± 11.2	9.1	118.6 ± 9.8	8.3	129.9 ± 7.2	5.6	129.9 ± 7.2	7.0
		3	116.4 ± 17.5	15.0	128.8 ± 12.0	9.3	125.9 ± 12.8	10.2	118.5 ± 12.3	10.3

CV = coefficient of variation, ROI = region of interest, SD = standard deviation

pronounced in the lower stiffness, agarose phantom.

For each machine, the inter-operator reproducibility (ICC [95% CI]) was 0.982 [0.976–0.986] for machine A and 0.985 [0.981–0.989] for machine B. The intra-operator reproducibility was 0.971 [0.962–0.977] for operator A and 0.960 [0.947–0.970] for operator B, indicating an excellent overall agreement.

DISCUSSION

In this study, we investigated the factors affecting the variability of transrectal SWE measurements using a designed phantom. Tissue equivalent US prostate phantoms are commercially available from Computerized Imaging Reference System (CIRS; Norfolk, VA, USA); however, most of these phantoms are designed for other imaging modalities or are usually available for linear or curved transducers (15). On the other hand, the designed phantom can assess the variability of transrectal SWE at different locations and can be manufactured with different sizes and shapes. Various soft tissue-mimicking materials have been used for imaging modalities and treatment planning (16, 17). The selection of phantom materials in this study was based on different stiffness properties which can mimic normal prostate and prostate cancer tissue. In general, the cancerous areas of the prostate have an average stiffness value between 58 and 90.5 kPa (18). The stiffness of silicone is usually two to three times

higher than Young's modulus of prostate cancer. Emulsion silicone exhibits better acoustic properties with less attenuation than pure silicone, as reported in the previous section. Agarose has variable stiffness depending on its concentration, and low-concentrated agar is known to have lower stiffness close to that of normal prostate tissue (19).

Until now, a few investigators have reported the reproducibility of SWE conducted on a commercial CIRS phantom with a linear or curved US transducer (20-25). In agreement with previous results (24, 25), we found that the variability gradually reduced with increasing phantom size. Fukuhara et al. (25) revealed that the SWE values are unstable when objects have small diameters. They attributed this to the fact that the US waves of the push pulse are reflected and refracted at the boundaries of the objects, which results in irregular production of shear waves. Alternatively, this attenuation might be associated with the background stiffness counting in a small phantom. We also found that the CV of the 2 cm inclusion was slightly lower than that of the 3 cm inclusion in some cases. This may have been related to the fact that the propagation of shear waves through the phantom material, especially in large regions, was more attenuated and led to a slight decrease in the mean SWE value in the large-sized phantom.

A few studies have demonstrated that measurement depth remarkably impacts variability (20-24), and the current study supports this finding. In our study, there was no significant difference in the SWE value obtained at different depths in most cases. However, the CV demonstrated an increasing tendency with depth. This could be due to the attenuation of the US beam at a higher depth, which results in a poor signal-to-noise ratio (20). In a study by Cao et al. (19) using a transrectal transducer, the measurements at a depth of 6.4 cm showed high variability, and the variability was reduced for depths of 5 cm or less. It is necessary to be cautious when interpreting the SWE values at higher depths using US transducers.

Several studies have reported significant differences in SWE measurements between machines (21, 23). Our study noted this with mean differences in SWE values between the two machines ranging from 3.42 to 21.95 kPa. In contrast, Seliger et al. (26) demonstrated no significant difference in SWE values between three machines (Acuson, EPIQ 7, and Apolio i500). In this study, the differences between the machines were more pronounced in the lower stiffness. The reason is not clear, but the large wavelength of displacement of field in softer phantom (27) could be attributed to inter-machine differences. Hence, caution is required when comparing the SWE results across different vendors in clinical practice.

Even though US is inherently operator dependent, our results support the reproducibility within inter- and intra-operator agreement of the SWE values (21, 28, 29). Lee et al. (28) reported an almost perfect reproducibility (ICC > 0.90) using a curved transducer. Mun et al. (29) assessed the intra- and inter-operator variability of SWE using a linear transducer which was highly reproducible across operators.

Our study had several limitations. First, this study did not evaluate a phantom material with intermediate stiffness. Second, the stiffness values of tissue-mimicking material were unclear, and it was assumed that the viscosity of the phantoms was homogeneous. Third, this phantom study did not consider other sources of variability that arise in clinical applications. Finally, our study included a small number of measurements which may have caused insufficient statistical power. Further studies with larger numbers of cases may yield statisti-

cally significant results.

In conclusion, the size of the phantom material, the depth from the transducer, and different machines were factors affecting the variability of transrectal SWE. Therefore, caution is needed when comparing SWE results across vendors.

Author Contributions

Conceptualization, all authors; data curation, L.J., Y.S.K.; formal analysis, all authors; investigation, L.J., Y.S.K.; methodology, all authors; project administration, L.J., Y.S.K.; resources, L.J., Y.S.K.; software, L.J., Y.S.K.; supervision, L.J.W., Y.S.K.; validation, L.J.W., Y.S.K.; visualization, L.J., Y.S.K.; writing—original draft, all authors; and writing—review & editing, all authors.

Conflicts of Interest

Seong Kuk Yoon has been an Section Editor of Journal of the Korean Society of Radiology since 2017; however, he was not involved in the peer reviewer selection, evaluation, or decision process of this article. Otherwise, no other potential conflicts of interest relevant to this article were reported.

Funding

REFERENCES

1. American Cancer Society. Prostate cancer. Atlanta, GA: American Cancer Society. Available at. https://www.cancer.org/cancer/prostate-cancer.html. Published 2021. Accessed July 11, 2022
2. Eichler K, Hempel S, Wilby J, Myers L, Bachmann LM, Kleijnen J. Diagnostic value of systematic biopsy methods in the investigation of prostate cancer: a systematic review. *J Urol* 2006;175:1605-1612
3. Ahmed HU, El-Shater Bosaily A, Brown LC, Gabe R, Kaplan R, Parmar MK, et al. Diagnostic accuracy of multi-parametric MRI and TRUS biopsy in prostate cancer (PROMIS): a paired validating confirmatory study. *Lancet* 2017;389:815-822
4. Pepe P, Fraggetta F, Galia A, Grasso G, Aragona F. Prostate cancer detection by TURP after repeated negative saturation biopsy in patients with persistent suspicion of cancer: a case-control study on 75 consecutive patients. *Prostate Cancer Prostatic Dis* 2010;13:83-86
5. Girouin N, Mège-Lechevallier F, Tonina Senes A, Bissery A, Rabilloud M, Maréchal JM, et al. Prostate dynamic contrast-enhanced MRI with simple visual diagnostic criteria: is it reasonable? *Eur Radiol* 2007;17:1498-1509
6. Langer DL, van der Kwast TH, Evans AJ, Trachtenberg J, Wilson BC, Haider MA. Prostate cancer detection with multi-parametric MRI: logistic regression analysis of quantitative T2, diffusion-weighted imaging, and dynamic contrast-enhanced MRI. *J Magn Reson Imaging* 2009;30:327-334
7. Beerlage HP, Aarnink RG, Ruijter ET, Witjes JA, Wijkstra H, Van De Kaa CA, et al. Correlation of transrectal ultrasound, computer analysis of transrectal ultrasound and histopathology of radical prostatectomy specimen. *Prostate Cancer Prostatic Dis* 2001;4:56-62
8. Hoyt K, Castaneda B, Zhang M, Nigwekar P, di Sant'agnese PA, Joseph JV, et al. Tissue elasticity properties as biomarkers for prostate cancer. *Cancer Biomark* 2008;4:213-225
9. Bercoff J, Tanter M, Fink M. Supersonic shear imaging: a new technique for soft tissue elasticity mapping. *IEEE Trans Ultrason Ferroelectr Freq Control* 2004;51:396-409
10. Ahmad S, Cao R, Varghese T, Bidaut L, Nabi G. Transrectal quantitative shear wave elastography in the detection and characterisation of prostate cancer. *Surg Endosc* 2013;27:3280-3287
11. Woo S, Kim SY, Cho JY, Kim SH. Shear wave elastography for detection of prostate cancer: a preliminary study. *Korean J Radiol* 2014;15:346-355
12. Boehm K, Budäus L, Tennstedt P, Beyer B, Schiffmann J, Larcher A, et al. Prediction of significant prostate cancer at prostate biopsy and per core detection rate of targeted and systematic biopsies using real-time shear wave elastography. *Urol Int* 2015;95:189-196
13. Chiu T, Xiong Z, Parsons D, Folkert MR, Medin PM, Hrycushko B. Low-cost 3D print-based phantom fabrica-

tion to facilitate interstitial prostate brachytherapy training program. *Brachytherapy* 2020;19:800-811

14. Lee DH, Lee JY, Bae JS, Yi NJ, Lee KW, Suh KS, et al. Shear-wave dispersion slope from US shear-wave elastography: detection of allograft damage after liver transplantation. *Radiology* 2019;293:327-333

15. Computerized Imaging Reference Systems. Multi-purpose, multi-tissue ultrasound phantom: model 040GSE. Norfolk, VA: Computerized Imaging Reference Systems. Available at. https://www.cirsinc.com/products/ultrasound/zerdine-hydrogel/multi-purpose-multi-tisse-ultrasound-phantom. Published 2013. Accessed June 13, 2022

16. D'Souza WD, Madsen EL, Unal O, Vigen KK, Frank GR, Thomadsen BR. Tissue mimicking materials for a multi-imaging modality prostate phantom. *Med Phys* 2001;28:688-700

17. King RL, Liu Y, Maruvada S, Herman BA, Wear KA, Harris GR. Development and characterization of a tissue-mimicking material for high-intensity focused ultrasound. *IEEE Trans Ultrason Ferroelectr Freq Control* 2011;58:1397-1405

18. Barr RG, Memo R, Schaub CR. Shear wave ultrasound elastography of the prostate: initial results. *Ultrasound Q* 2012;28:13-20

19. Cao R, Huang Z, Varghese T, Nabi G. Tissue mimicking materials for the detection of prostate cancer using shear wave elastography: a validation study. *Med Phys* 2013;40:022903

20. Palmeri M, Nightingale K, Fielding S, Rouze N, Deng Y, Lynch T, et al. RSNA QIBA ultrasound shear wave speed phase II phantom study in viscoelastic media. Proceedings of the 2015 IEEE International Ultrasonics Symposium (IUS); 2015 Oct 21-24; Taipei, Taiwan: IEEE; 2015; p.1-4

21. Alrashed AI, Alfuraih AM. Reproducibility of shear wave elastography among operators, machines, and probes in an elasticity phantom. *Ultrasonography* 2020;40:158-166

22. Hwang J, Yoon HM, Jung AY, Lee JS, Cho YA. Comparison of 2-dimensional shear wave elastographic measurements using ElastQ imaging and SuperSonic shear imaging: phantom study and clinical pilot study. *J Ultrasound Med* 2020;39:311-321

23. Shin HJ, Kim MJ, Kim HY, Roh YH, Lee MJ. Comparison of shear wave velocities on ultrasound elastography between different machines, transducers, and acquisition depths: a phantom study. *Eur Radiol* 2016;26:3361-3367

24. Hwang JA, Jeong WK, Song KD, Kang KA, Lim HK. 2-D shear wave elastography for focal lesions in liver phantoms: effects of background stiffness, depth and size of focal lesions on stiffness measurement. *Ultrasound Med Biol* 2019;45:3261-3268

25. Fukuhara T, Matsuda E, Fujiwara K, Tanimura C, Izawa S, Kataoka H, et al. Phantom experiment and clinical utility of quantitative shear wave elastography for differentiating thyroid nodules. *Endocr J* 2014;61:615-621

26. Seliger G, Chaoui K, Kunze C, Dridi Y, Jenderka KV, Wienke A, et al. Intra- and inter-observer variation and accuracy using different shear wave elastography methods to assess circumscribed objects - a phantom study. *Med Ultrason* 2017;19:357-365

27. Korta Martiartu N, Nambiar S, Nascimento Kirchner I, Paverd C, Cester D, Frauenfelder T, et al. Sources of variability in shear wave speed and dispersion quantification with ultrasound elastography: a phantom study. *Ultrasound Med Biol* 2021;47:3529-3542

28. Lee SM, Chang W, Kang HJ, Ahn SJ, Lee JH, Lee JM. Comparison of four different shear wave elastography platforms according to abdominal wall thickness in liver fibrosis evaluation: a phantom study. *Med Ultrason* 2019;21:22-29

29. Mun HS, Choi SH, Kook SH, Choi Y, Jeong WK, Kim Y. Validation of intra- and interobserver reproducibility of shearwave elastography: phantom study. *Ultrasonics* 2013;53:1039-1043

팬텀연구에서 경직장 전단파탄성초음파의 가변성

이지현[1] · 윤성국[2]* · 조진한[2] · 권희진[2] · 김동원[3] · 이준우[4]

목적 본 연구는 제작한 팬텀을 사용해 경직장 전단파탄성초음파의 가변성을 알아보았다.

대상과 방법 아가로즈와 실리콘에멀전을 각각 1, 2, 3 cm 크기의 둥근 모양과 사각 모양의 팬텀 물질로 제작하였다. 1, 2, 3 cm의 깊이에 팬텀을 놓고, 크기, 깊이, 모양에 따른 굳기값(coefficient variant)의 차이를 중심부/주변부에서 확인하였다. 두 명의 영상의가 경직장 초음파 탐촉자를 이용해 각각 3회씩, 두 개의 초음파기계로(기계 A, B), 굳기값을 확인하였다. 가변성은 변동계수로 표현하였다.

결과 팬텀의 크기가 커질수록 변동계수는 감소하였다. 크기에 따른 굳기값은, 아가로즈 팬텀은 기계 A 3 cm 깊이($p < 0.001$), 기계 B 1 cm 깊이에서($p = 0.010$), 실리콘에멀전 팬텀은 2 cm 깊이에서 두 기계 모두 유의한 차이를 보였다($p = 0.047$, $p = 0.020$). 깊이가 깊어질수록 변동계수는 증가하였다. 깊이에 따른 굳기값은, 1 cm 크기 아가로즈 팬텀은 두 기계 모두($p = 0.037$, $p = 0.021$), 2 cm 크기 아가로즈 팬텀은 기계 A에($p = 0.047$) 유의한 차이를 보였다. 기계 A 실리콘에멀전에서만 모양에 따른 굳기값의 유의한 차이를 보였고($p = 0.032$) 기계 B는 두 물질 모두 관심영역에 따른 굳기값의 유의한 차이가 보였다. 굳기값은 두 기계 간 유의한 차이가 있었고($p < 0.05$), 시술자 내/시술자 간 일치도는 높았다(급내상관계수 > 0.9).

결론 팬텀의 크기, 깊이, 사용된 기계가 전단파탄성초음파 가변성에 영향을 주는 요소로 나타났다.

[1]동남권원자력의학원 영상의학과,
[2]동아대학교 의과대학 동아대학교병원 영상의학과,
[3]이샘병원 영상의학과,
[4] 양산부산대학교병원 영상의학과